SCIENCE CHINA Materials ARTICLES

mater.scichina.com link.springer.com

Published online 12 March 2018 | https://doi.org/10.1007/s40843-017-9224-x
Sci China Mater 2018, 61(8): 1085–1094

Cu_xO self-assembled mesoporous microspheres with effective surface oxygen vacancy and their room temperature NO_2 gas sensing performance

Siyuan Li[†], Mengting Wang[†], Chaozheng Li, Jiajia Liu[*], Meng Xu, Jia Liu and Jiatao Zhang[*]

ABSTRACT **A series of Cu_xO self-assembled mesoporous microspheres (SMMs), with different and controlled morphology (virus-like, urchin-like, spherical), were synthesized by facile liquid phase approach. The morphology of the as-prepared Cu_xO SMMs was evolved from spherical to virus-like shape by controlling the ratio of DI water in solution. It can also realize the transformation from loose assembly to dense assembly by extending the reaction time. These Cu_xO SMMs exhibited good response to NO_2 gas at room temperature, benefiting from their 3D self-assembly structure. Among these the resulting virus-like Cu_xO SNMMs-based sensor exhibits largely enhanced response to 1 ppm NO_2 gas at room temperature. The enhanced response of the virus-like Cu_2O SMMs-based sensor can be ascribed to the high surface area, hierarchical 3D nanostructures, micropores for effective gas diffusion, the heterojunctions formed between CuO and Cu_2O, and the existence of abundant surface oxygen vacancies.**

Keywords: self-assembly, mesoporous, Cu_xO, oxygen vacancy, NO_2 gas sensing

INTRODUCTION

The assembly of nanoparticles has emerged as an alternative approach to utilize and exploit nanomaterials in a scalable manner [1]. These nanostructures from assembly of nanoparticles represent a new class of potential building blocks for making functional materials, because they have additional collective properties induced by coupling between their constituents as well as the chemical and physical properties inherited from their constituent nanoparticles [2,3]. Numerous two-dimensional (2D) and three-dimensional (3D) super-nanostructures based on assembled nanoparticles have been fabricated for applications in sensing, photonics, optoelectronics, photovoltaics and electronic devices [4–6]. For example, the assemblies of metal nanoparticles have advantages in molecular detection by surface-enhanced Raman scattering in comparison to the individual nanoparticles [7]. 3D multilayer superlattices film has a much higher rate of photocurrent generation han that of its disordered-assembled counterpart [8]. Mesoporous colloidal superparticles made of platinum-group nanocrystals show significantly improved catalytic activity and recyclability in catalyzing solution-phase electron-transfer reactions in comparison with the well-dispersed small Pt nanocrystals [9]. Therefore, the assembly of inorganic nano-building blocks into complex 3D superstructures with well-controlled porosity, morphologies and surface defect states is still an incipient area and in strong demand.

Detection of polluted air is important for environmental monitoring, personal safety protection, and industrial manufacturing nowadays. Nitrogen dioxide (NO_2) is a notorious gas mainly released from vehicle exhausts and fossil fuel combustion, which threatens the environment and causes respiratory problems in human beings [10]. However, traditional NO_2 gas sensors are usually operated between 200 and 400°C, since closely packed metal oxides have high resistance at room temperature [11–14]. Various efforts have been devoted to decreasing the operation temperature, such as tuning the morphology of the nanostructures, surface modification, and fabrication of hybrid or composite nanostructures. For example, tungsten oxide (WO_3) hollow spheres exhibited good response to 100 ppb NO_2 at 140°C due to their hierarchical self-assembled structure [15]. The sensors based on concave Cu_2O octahedral nanostructure

Beijing Key Laboratory of Construction-Tailorable Advanced Functional Materials and Green Applications, School of Materials Science & Engineering, Beijing Institute of Technology, Beijing 100081, China
[†] These authors contributed equally to this work.
[*] Corresponding authors (emails: zhangjt@bit.edu.cn (Zhang J); liujiajia@bit.edu.cn (Liu J))

had good sensing response to NO_2 at 50°C due to their unique concave octahedral-shape [16]. Nickel oxide (NiO) hexagonal nanosheets with micropores present good sensitivity to NO_2 at room temperature due to the abundant nickel vacancies formed in NiO [17]. Tin oxide (SnO_2) nanoflower-based sensor exhibited high response toward 200 ppb NO_2 at room temperature due to the oxygen vacancies [18]. Also Cu_2O nanocrystals/graphene composites exhibited an excellent sensitivity toward NO_2 at room temperature [19,20]. The good room temperature sensing performance was attributed to the improved conductivity and effective gas diffusion. Therefore, the metal-oxide-based gas sensors could realize room temperature gas sensing if the sensing materials are elaborately designed with well-controlled porosity, nanoscale structure and surface defect states.

In the present study, a series of Cu_xO self-assembled mesoporous microspheres (SMMs), with different and controlled morphology (virus-like, urchin-like, spherical), were synthesized by a facile liquid method. The morphological and 3D self-assembly structural properties of the as-prepared Cu_xO SMMs were studied in detail. Their surface area, porosity, and surface oxygen vacancies have been analyzed by the nitrogen adsorption-desorption isotherm curves, electron paramagnetic resonance (EPR) and X-ray photoelectron spectroscopy (XPS) spectra. These Cu_xO SMMs are shown to perform effectively as sensing material for NO_2 gas at room temperature. Furthermore, the underlying gas sensing mechanism for the enhanced response characteristics due to the 3D self-assembled Cu_xO SMMs is also discussed.

EXPERIMENTAL SECTION

Materials

All reagents were of analysis grade and were used without further treatment. The Cu_2O SNMMs were prepared following an approach by Zhang *et al.* [21] with a minor modification of reactant content. 0.4 g copper acetate ($(CH_3COO)_2Cu{\cdot}H_2O$) (Sinopharm) was dissolved in 30 mL *N*,*N*-dimethylformamide (DMF) (Beijing chemical reagent factory, containing ~0.1% water), followed by the addition of poly(vinyl pyrrolidone) (PVP, 0.165 g, molecular weight = 30,000) (Sinopharm), and 0–0.5 mL deionized (DI) water. After stirring for several minutes, 40 mg $NaBH_4$ (Tianjin Fuchen Chemical reagent factory) was added. The mixture was heated to 80°C for 2–6 min. Drastic changes in the liquid color were observed during reduction of Cu^{2+} to Cu^{+} (blue to green to light yellow) quickly. Once the color of the mixture changed to light yellow, the mixture was dipped into the water bath to cool down. The precipitate was centrifuged, washed with ethanol several times.

Material characterizations

The morphologies of the as-synthesized samples were examined on SIRION 200 field emission scanning electron microscope (FESEM), and JEOL JEM-1200EX transmission electron microscope (TEM) (Hitachi H-7650B) at 100.0 kV. High resolution TEM was recorded on Tecnai G2 F20 S-Twin, operating at 200.0 kV. X-ray diffraction (XRD) patterns of the as-obtained product were recorded on a Bruker D8 Advance powder X-ray diffractometer at a scanning rate of 2° min^{-1}, using Cu-Kα radiation (λ=1.5406 Å). X-ray photoelectron spectroscopy (XPS) spectra were obtained with a PHI Quantera II XPS system using Al Kα non-monochromatic radiation. The measurement parameters were: light spot size: 100 μm; power: 100 W; voltage: 20 kV. Measurements of Brunauer-Emmett-Teller (BET) surface area and porosity were carried out at 77 K with a Quantachrome Instrument ASiQMVH002-5 system. Electron paramagnetic resonance (EPR) experiments were performed on a Bruker EMX X-band spectrometer and microwave frequency=9.40 GHz at room temperature.

NO_2 gas sensing performance evaluation

First, the gas sensor was fabricated by putting slurry of as-prepared Cu_xO SMMs on the cleaned alumina substrates which were attached with a pair of interdigital Pt electrodes and followed by a thermal treatment at 200°C for 2 h in order to burn out the organic solvent used in the preparation of coating slurry and to enhance the adherence of the sensing film to the sensor substrate. The target gas concentration was controlled by injecting volume of the target gas [22]. For recovery of the sensor resistance, the testing chamber was open in air. The changes of the sensor resistance in air or target gas were monitored by a gas sensing testing system (WS-30A, Winsen, China). The gas responses ($S=R_a/R_g$ for oxidizing gas or R_g/R_a for reducing gas, R_a: resistance in the atmospheric air, R_g: resistance in the target gas) to NO_2, SO_2, C_2H_5OH, $C_6H_5CH_3$, $(CH_3)_2CO$, CH_3OH, C_3H_7NO were measured at room temperature (25°C, humidity 26%).

RESULTS AND DISCUSSION

Fig. 1 and Fig. S1 (see Supplementary information) show the FESEM images of the resulting Cu_xO SMMs with different morphologies synthesized by the liquid phase

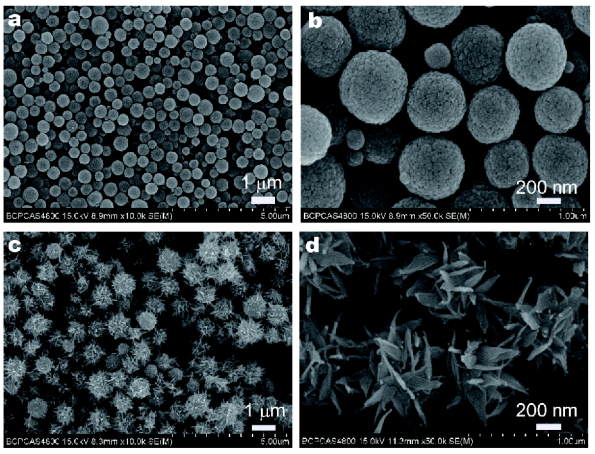

Figure 1 FESEM images of the as-synthesized different Cu_xO SMMs with different amount of H_2O: (a, b) spherical Cu_xO SMMs (0.1–0.2 mL); (c, d) virus-like Cu_xO SMMs (~0.5 mL).

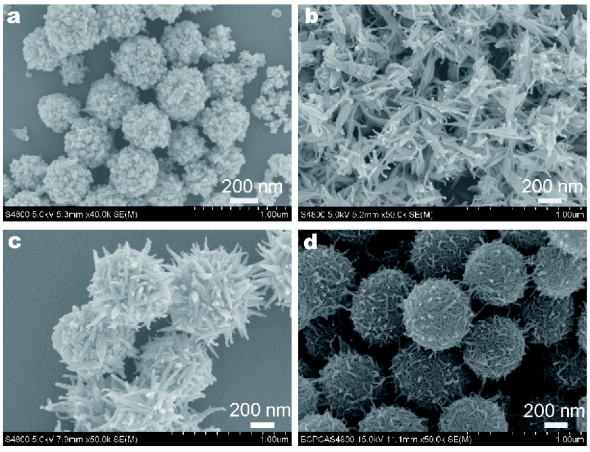

Figure 2 (a) FESEM images of the spherical Cu_xO SMMs obtained at 1–2 min after the mixture was heated to 80°C (0.1–0.2 mL H_2O), (b–d) FESEM images of the as-synthesized virus-like Cu_xO SMMs obtained at different reaction time (~0.5 mL H_2O) (b) 1–2 min, (c) ~5 min, (d) ~6 min.

approach with different amount of DI water in DMF solution. It shows the interesting morphology evolution from spherical to virus-like Cu_xO SMMs. In the presence of 0.1–0.2 mL of H_2O (in 30 mL DMF), spherical Cu_xO SMMs with diameters of approximately 500 nm are formed. When the amount of water is increased to 0.5 mL, the FESEM images (Fig. 1c, d) indicate that the virus-like Cu_xO SMMs with a diameter approximately 0.7 μm are composed of fusiform nanorods building blocks.

Generally, the growth process of crystals is a kinetically and thermodynamically controlled process. The formation process of these Cu_xO SMMs with shape evolution was examined by observing the intermediate structures formed after the mixture was heated to 80°C for about 2 min (Fig. 2a, b). For spherical Cu_xO SMMs (Fig. 2a), nanoparticles with rough surface but overall spherical morphologies appeared. These intermediate structures seem to be formed through aggregation of smaller crystals 30–60 nm in diameter. For virus-like Cu_xO SMMs, at the early stage (~2 min) (Fig. 2b), the product is composed of fusiform rods, which seems to result from the assembling with nanorods with diameter of 20–30 nm. Extending the reaction time to 3–4 min, loosely packed virus-like aggregates of Cu_2O SMMs from the preformed fusiform rods were formed as shown in Fig. 1c, d. Further extending the reaction time to 5–6 min (before the color of solution gets dark), it seems that the aggregates become more compact (Fig. 2c) to the urchin-like Cu_xO SMMs (Fig. 2d).

The phase and purity of the as-synthesized three Cu_xO SMMs were characterized by powder XRD measurements. As shown in Fig. 3a, all the diffraction peaks can be indexed to cuprite Cu_2O (JCPDS No. 05-0667). No characteristic peaks corresponding to impurities are found, showing the high purity of the sample. Moreover, the spherical Cu_xO SMMs have a higher intensity and smaller full width at half maxim (FWHM) than the urchin-like and virus-like Cu_xO SMMs, indicating that the crystallinity of the spherical Cu_xO SMMs is higher. The phase purity of as-synthesized Cu_xO SMMs was further examined by EPR technique and shown in Fig. 3b. As reported, Cu^+ ions are diamagnetic ($3d^{10}$) and therefore EPR silent [23]. Cu^{2+} ions, on the contrary, have an electron configuration of d^9 and are paramagnetic over a wide range of temperatures [24]. The resonance peaks have been observed in the virus-like Cu_xO SMMs (curve C) which could be assigned to the paramagnetic Cu^{2+} ions. While for the urchin-like Cu_xO SMMs, the EPR signal of Cu^{2+} cations almost disappeared (curve B), indicating the majority of the EPR-silent low-valence Cu^+. However, the spectrum of the spherical Cu_xO SMMs is composed of two broad signals (curve A). At room temperature, the observed resonance signal is assigned to the paramagnetic Cu^{2+} ions. The broadness of the resonance peak is attributed to the superposition of closely spaced peaks of Cu^{2+} ions [25]. The peak shift to the left for the spherical Cu_xO SMMs may be attributed to the relative low concentration of Cu^{2+} cations, in agreement with XPS evidence for the presence of copper in the Cu^{2+} oxidation [26]. EPR studies show that CuO is present in

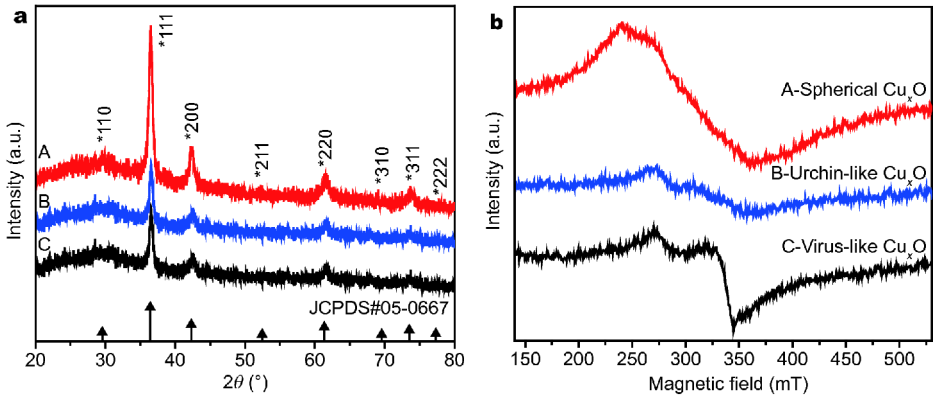

Figure 3 (a) XRD patterns of the three types of Cu_xO SNMMs, A) spherical Cu_xO SMMs, B) urchin-like Cu_xO SMMs, C) virus-like Cu_xO SMMs. (b) EPR spectra of the three types of Cu_xO SMMs, A) spherical Cu_xO SMMs, B) urchin-like Cu_xO SMMs, C) virus-like Cu_xO SMMs.

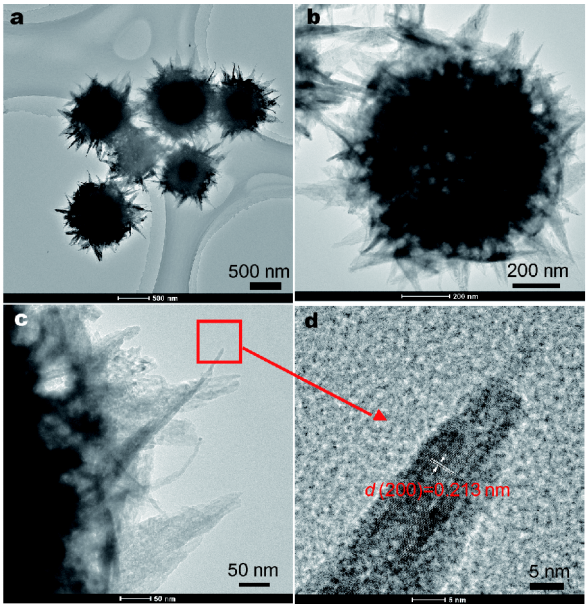

Figure 4 (a–d) HRTEM images of the virus-like Cu_xO SMMs.

the as-synthesized Cu_2O SMMs. XRD studies show only Cu_2O phase, which means that CuO could be in the non-crystalline form. From these results, we conclude that the as-synthesized Cu_xO SMMs consist of multiphase like CuO and Cu_2O.

A morphology resembling fusiform rods is also evident from the HRTEM image of a single virus-like Cu_xO SMMs (Fig. 4). The well-defined virus-like Cu_xO SMMs with a diameter of about 0.7 μm show puffy 3D network structures assembled with many fusiform rods (Fig. 4b). An HRTEM image of the edge area of the virus-like Cu_xO SMMs is shown in Fig. 4d. The lattice fringe of $d_{(200)}$ was measured at about 2.13 Å, which is in good agreement with 2.12 and 2.14 Å in the literature [27].

The redox chemical process for the formation of the Cu_2O phase in DMF-water solvent system had been proposed in our previous work [21], where the solid Cu_2O nanospheres (~200 nm) without porosity were synthesized. In this work, more loose hierarchical 3D assembled Cu_xO microspheres with higher surface area and mesopores were achieved. $NaBH_4$, as a strong reducing agent, reacts with hydroxyl ion of water and releases electrons. In the first step of the reaction, Cu^{2+} ions accept this electron to form Cu^+ ions. The Cu^+ ions in the presence of water finally lead to the formation of primary Cu_2O nanocrystals. With increasing amount of water, the reaction kinetics could be flexibly tuned, thus leading to increasing reaction rate, and the enhancement of supersaturation of primary Cu_2O nanocrystal building blocks. With the small amount of water (0.1–0.2 mL H_2O) and the synergistic effect from DMF solvent and PVP stabilization agents, the primary Cu_2O nanocrystals prefer to aggregate into spherical nanospheres [28]. Increasing the amount of water to 0.5 mL, fusiform rods were formed. With extended reaction time, virus-like and urchin-like Cu_xO SMMs were formed through the aggregation of fusiform rods. From the above complementary analyses, it can be understood that the formation process of three hierarchical Cu_xO SMMs were formed with the following steps (Scheme 1): i) production of primary Cu_xO nanocrystallites, ii) self-aggregation of primary Cu_xO nanocrystallites to spherical-shaped structures (0.1–0.2 mL H_2O) or fusiform rods (0.5 mL H_2O), iii) further growth to spherical Cu_xO SMMs, or virus-like Cu_xO SMMs (urchin-like Cu_xO SMMs).

Gas sensing is a kind of surface phenomenon, which

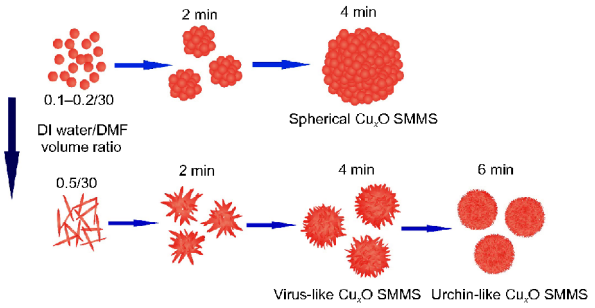

Scheme 1 Schematic illustration of the proposed mechanism for the formation of Cu$_x$O SMMs with various morphologies.

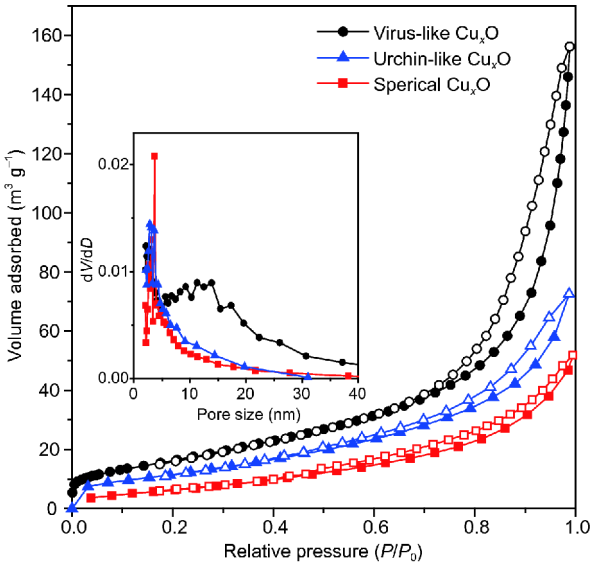

Figure 5 Nitrogen adsorption-desorption isotherms of different Cu$_x$O SMMs. The inset shows the BJH pore size distribution plots.

involves gas-solid interaction that occurs at the sensor surface. Therefore, their performance is governed by the exposed surface area, which means increasing the active surface area will likely increase the sensor performance. As shown from the nitrogen adsorption and desorption curves of the three Cu$_x$O SMMs in Fig. 5, the three Cu$_x$O SMMs show a type III isotherm. There is a H3-type hysteresis loop over a relative pressure range of 0.7–1.0, which is usually attributed to the slit like pores of the aggregates (loose assemblages) of primary particles [29]. According to the multiple BET measurements, the specific surface areas of the three Cu$_x$O SMMs are 68.30, 44.23 and 28.71 m^2 g^{-1} for the virus-like, urchin-like, and spherical Cu$_x$O SMMs, respectively (Table 1). The pore size distribution of these samples is shown in the inset of Fig. 5. The virus-like Cu$_x$O SMMs have two pore size

Table 1 Surface area, BJH pore size, and total pore volume of Cu$_x$O SMMs

	Surface area (m^2 g^{-1})	Pore size (nm)	Total pore volume (cm^3 g^{-1})
Spherical	28.71	3.14	0.10
Urchin-like	44.23	4.63	0.12
Virus-like	68.30	2.20, 12.26	0.29

distributions with the maximum peaks at 1.7 and 12 nm, respectively. In contrast, the urchin-like and spherical Cu$_x$O SMMs have pore size distributions with the maximum peaks at 4.33 nm and 3.29 nm, respectively. Obviously, the high specific surface area of the virus-like Cu$_x$O SMMs is attributed to the loose aggregation of fusiform rods.

Besides the specific surface area, the surface state of sensing materials, depending upon the adsorbent species, plays key roles in gas sensing [30]. The surface property of the as-prepared Cu$_x$O SMMs was studied by the XPS spectra. Fig. 6a shows the main and the satellite peaks of Cu $2p_{3/2}$ and Cu $2p_{1/2}$ of the as-prepared Cu$_x$O SMMs. The peak position and relative intensities of the satellites from these levels are indicative of the presence of CuO at the surface [31,32]. Therefore, both the CuO and Cu_2O coexist on the surface of the as-prepared Cu$_x$O SMMs. Fig. 6b–d show the O 1s XPS spectra of the as-prepared Cu$_x$O SMMs, which can be deconvoluted into four peaks with binding energies of ~529.6, ~530.3, ~531.2, and ~532.0 eV, corresponding to the binding states of Cu^{2+} ($O_L(Cu^{2+})$), Cu^+ ($O_L(Cu^+)$), oxygen vacancy (O_V), and adsorbed oxygen (O_C) [30]. The O_C component is usually attributed to chemisorbed and dissociated oxygen species (O_2^-, O^{2-} or O^-) and OH^-. The relative proportion of O_C in the as-prepared Cu$_x$O SMMs is 11.44%, 7.96%, 12.99% for the virus-like, urchin-like, and spherical Cu$_x$O SMMs (Table 2). In addition, it is observed that the percentage of O_V in the as-prepared Cu$_x$O SMMs is 17.38%, 13.77%, and 13.90% for the virus-like, urchin-like, and spherical Cu$_x$O SMMs (Table 2).

To study gas sensing applications of the as-prepared Cu$_x$O SMMs, their sensing performances against NO_2 are exhibited in the concentration range of 1–20 ppm at room temperature and 1 ppm N_2O at different temperatures (Fig. S2), and the dynamic response-recovery curves are shown in Fig. 7a. The sensor resistances decreased with the exposure of NO_2, indicating the p-type response of the sensor [16]. During the exposure of NO_2 the sensitivities of all three devices increase with increasing gas concentration due to the similar p-type

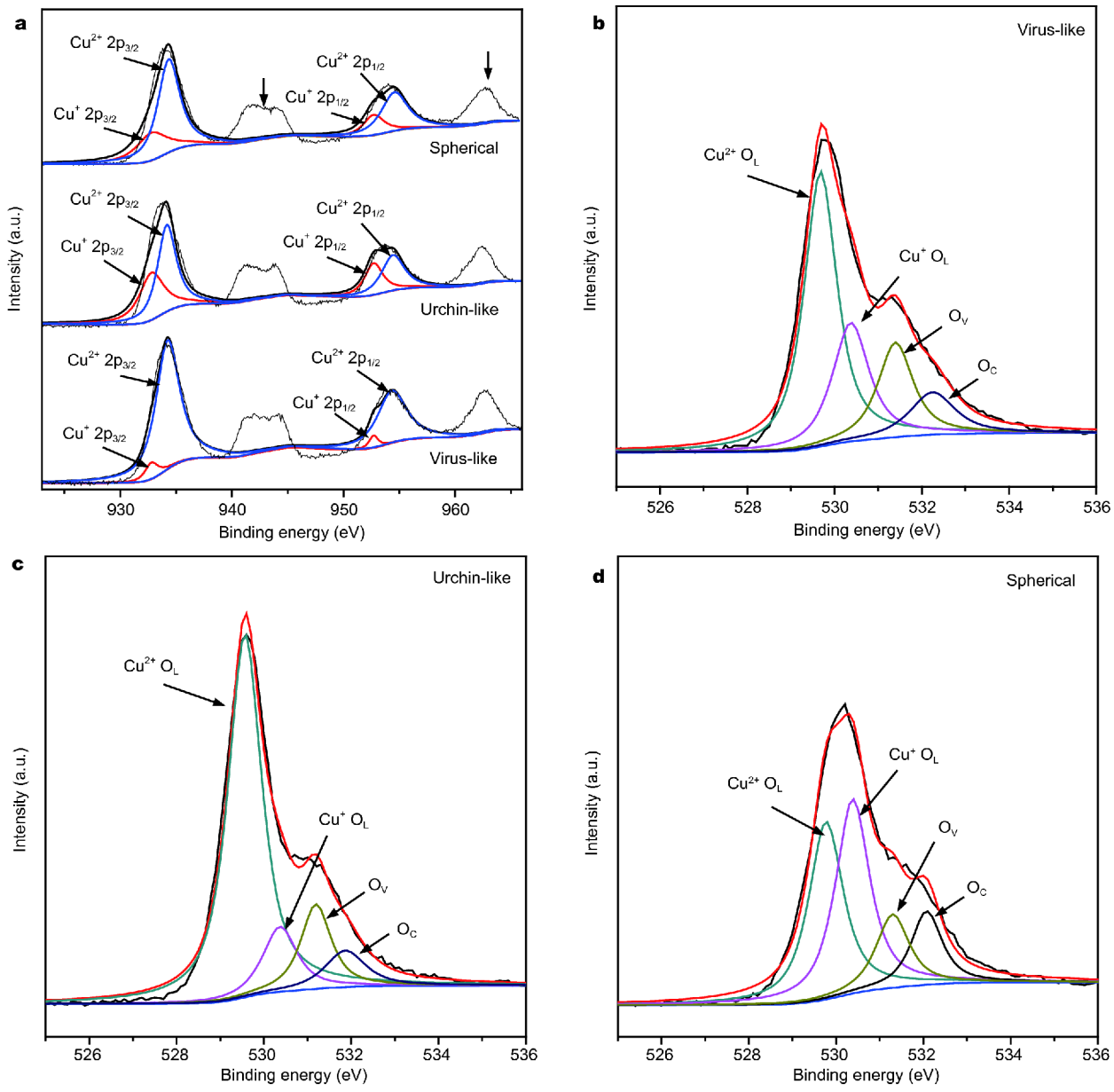

Figure 6 (a) Cu 2p XPS spectra and (b–d) O 1s XPS spectra of the three Cu_xO samples: (b) virus-like, (c) urchin-like, (d) spherical Cu_xO SMMs.

nature of Cu_xO SMMs (Fig. 7b). Moreover, the sensor response towards 4 ppm NO_2 for five successive cycles maintained at a similar value (Fig. S3). It is well-known that the gas sensing by semiconductor metal oxides involve two major key steps: the recognition of a target gas through a gas-solid interface which induces an electronic change of the oxide surface, and the transduction of the surface phenomenon into an electrical resistance change of the sensor [14]. All the Cu_xO SMMs exhibited the room temperature gas sensing ability, which could be ascribed to the large amount of oxygen vacancies, and the high specific surface area resulting from their 3D self-assembly structure. Recent theoretical and experimental studies have demonstrated that the sensor performance of metal oxides is related to the presence of oxygen-vacancy (O_V) defects, which can serve as the adsorption sites and facilitate the chemisorption of oxygen at low temperature [18,33]. Meanwhile, it is reported that the presence of O_V defects on Cu_xO can serve as trapping sites for grabbing reactant molecules, thus further improving the catalytic

Table 2 Fitting results of O 1s XPS spectra of the Cu_xO SMMs

	Oxygen species	Binding energy (eV)	Relative percentage (%)
Virus-like	$O_L(Cu^+)$	529.68	48.45
	$O_L(Cu^{2+})$	530.37	22.73
	O_V (vacancy)	531.36	17.38
	O_C (chemisorbed)	532.19	11.44
Urchin-like	$O_L(Cu^+)$	529.57	66.38
	$O_L(Cu^{2+})$	530.37	11.89
	O_V (vacancy)	531.19	13.77
	O_C (chemisorbed)	531.86	7.96
Spherical	$O_L(Cu^+)$	529.77	35.01
	$O_L(Cu^{2+})$	530.38	38.10
	O_V (vacancy)	531.29	13.90
	O_C (chemisorbed)	532.07	12.99

activity of Cu_xO [34]. Therefore, the existence of rich oxygen vacancies may be particularly preferable for NO_2 adsorption, hence improving sensing performance of the Cu_xO SMMs.

Among the three samples, the virus-like Cu_xO SMMs perform the best, and the gas responses (R_a/R_g, R_a: resistance in air, R_g: resistance in gas) to 1, 2, 4, 8, and 16 ppm NO_2 were about 8.7, 16.6, 28.4, 38.6, and 56.1, respectively. The response time (t_{res}), corresponding to the time reaching the 90% steady response and the recovery time (t_{rec}), corresponding to the time attaining 10% of the initial response, were determined. The t_{res} and t_{rec} upon exposure to 4 ppm NO_2 for the virus-like Cu_xO SMMs based sensor were 22 s and 42 s, respectively, which are faster than those observed in the previous study for NO_2 (Table S1, Supplementary information)

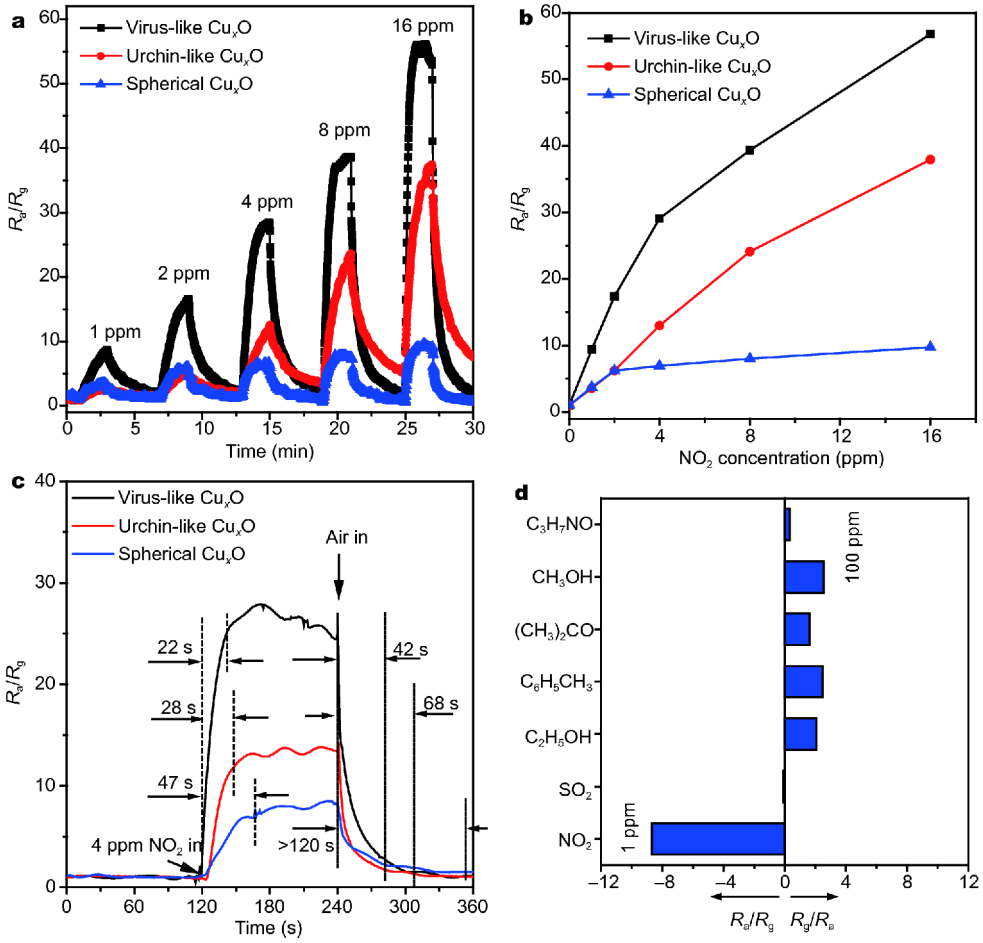

Figure 7 (a) Dynamic response-recovery curves of the different Cu_xO SMMs to different concentrations of NO_2 at room temperature (25°C, humidity 26%). (b) Gas responses for NO_2 as a function of concentration recorded at room temperature (25°C, humidity 26%). (c) Response curves for 4 ppm NO_2 at room temperature in order to calculate the t_{res} and t_{rec} times (25°C, humidity 26%). (d) Gas response (R_a/R_g or R_g/R_a) of the virus-like Cu_xO SMMs to 1 ppm NO_2 and 100 ppm SO_2, C_2H_5OH, $C_6H_5CH_3$, $(CH_3)_2CO$, CH_3OH, C_3H_7NO (25°C, humidity 26%).

[17,18,22]. We also measured the response of virus-like Cu_xO SMMs based sensor to some typical combustible and toxic gases. Fig. 7d compares the response of the sensor to various gases including sulfur dioxide, ethanol, toluene, acetone, methanol at room temperature. The virus-like Cu_xO SMMs exhibit the largest response and superior selectivity to NO_2 against other tested gases at room temperature. On the basis of our experimental results, morphology seems to be a key factor to control the gas-sensing performance. In particular, the enhanced gas-sensing properties of virus-like Cu_xO SMMs are likely to result from the following reasons. First, the gas sensing properties in the oxide-based materials are largely governed *via* surface reactions and through the diffusion of the target gases [14]. The surface area for gas sensing in hierarchical structures is determined by the dimensions and packing configuration of building blocks. The enhanced gas-sensing properties of virus-like Cu_xO SMMs may be ascribed to their unique loosely assembled structure, which provides well-defined porosity for effective gas diffusion. In the compact aggregates structure (urchin-like, spherical Cu_xO SMMs), the surface area and pore size decrease, which hampers the diffusion of target gases toward the inner part of the secondary particles. Second, the behavior of metal oxide based sensor to gases is based on changes in electric resistance induced by adsorption/desorption of detection gas on its surface. The results of EPR and XPS have found that the as-prepared Cu_xO SMMs have thin layer of CuO on the surface. Both conduction band and valence band of Cu_2O are situated below those of CuO (Fig. S4) [35,36]. When the sensor is exposed to air, oxygen molecules would be adsorbed on the surface of the virus-like Cu_xO SMMs to generate oxygen ions (O_2^-, O^{2-} or O^-), leading to the increase of hole concentration and the decrease of the resistance. NO_2 has an unpaired electron as a stronger oxidizer than oxygen. When the sensor film is exposed to NO_2 gas at room temperature, NO_2 can not only capture the electrons from the valence band due to its higher electrophilic properties but also react with the pre-adsorbed oxygen species (O_2^-) leading to the formation of adsorbed NO_2^- (ads) and O^- (ads). The above reactions decrease the electron concentration on the surface of the virus-like Cu_xO SMMs and promote the hole conductivity in the virus-like Cu_xO SMMs, which results in a decrease of the resistance. Additionally, the hole will also transfer from the CuO layer on the surface to the inner Cu_2O layer, thus forming a heterojunction barrier and an additional depletion layer at the interface (Fig. S4), which greatly decreases the sensor resistance of the virus-like Cu_xO SMMs. After NO_2 gas is removed, the resistance returns to the original value due to the re-adsorption of oxygen. The enhanced sensing performance of the virus-like Cu_xO SMMs is partly attributed to the heterojunctions formed between Cu_2O and CuO [23–26]. Third, the percentage of oxygen vacancy of the virus-like Cu_xO SMMs is higher than that of the other Cu_xO SMMs. From all the above discussion, the high performance of the virus-like Cu_xO SMMs gas sensors for NO_2 can be ascribed to the high surface area, hierarchical nanostructures, effective gas diffusion of pore, mixed valence states of Cu and the existence of rich oxygen vacancies.

CONCLUSION

In summary, Cu_xO SMMs with different and controlled morphology (virus-like, urchin-like, spherical) have been successfully synthesized by a facile liquid phase approach. Their 3D superstructures evolved from spherical to virus-like SMMs with flexible porosities by controlling the ratio of DI water in solution. In particular, such method could enable abundant oxygen vacancies on the surface of as-prepared Cu_xO SMMs. Due to their high surface area, hierarchical nanostructures, effective gas diffusion of pore, the heterojunctions formed between CuO and Cu_2O, and the existence of rich oxygen vacancies, these Cu_xO SMMs exhibit enhanced NO_2 sensing performance at room temperature. The synergistic effect of metal oxide super-nanostructures with single-layer level surface control to get enhanced catalytic gas sensing here are potential for guiding more transitional metal oxide nano-building blocks synthesis and applications.

Received 24 November 2017; accepted 30 January 2018; published online 12 March 2018

1 Zhu J, Hersam MC. Assembly and electronic applications of colloidal nanomaterials. Adv Mater, 2017, 29: 1603895
2 Yan C, Wang T. A new view for nanoparticle assemblies: from crystalline to binary cooperative complementarity. Chem Soc Rev, 2017, 46: 1483–1509
3 Bian Z, Tachikawa T, Zhang P, *et al.* A nanocomposite superstructure of metal oxides with effective charge transfer interfaces. Nat Commun, 2014, 5: 3038
4 Yang J, Choi MK, Kim DH, *et al.* Designed assembly and integration of colloidal nanocrystals for device applications. Adv Mater, 2016, 28: 1176–1207
5 Nosheen F, Zhang Z, Xiang G, *et al.* Three-dimensional hierarchical Pt-Cu superstructures. Nano Res, 2015, 8: 832–838
6 Wu Y, Wang D, Li Y. Understanding of the major reactions in solution synthesis of functional nanomaterials. Sci China Mater, 2016, 59: 938–996
7 Romo-Herrera JM, Alvarez-Puebla RA, Liz-Marzán LM. Controlled assembly of plasmonic colloidal nanoparticle clusters. Nanoscale, 2011, 3: 1304–1315

8 Huang L, Zheng J, Huang L, *et al.* Controlled synthesis and flexible self-assembly of monodisperse Au@semiconductor core/shell hetero-nanocrystals into diverse superstructures. Chem Mater, 2017, 29: 2355–2363
9 Hu Y, Liu Y, Sun Y. Mesoporous colloidal superparticles of platinum-group nanocrystals with surfactant-free surfaces and enhanced heterogeneous catalysis. Adv Funct Mater, 2015, 25: 1638–1647
10 Gurlo A. Nanosensors: towards morphological control of gas sensing activity. SnO_2, In_2O_3, ZnO and WO_3 case studies. Nanoscale, 2011, 3: 154–165
11 Yuan W, Huang L, Zhou Q, *et al.* Ultrasensitive and selective nitrogen dioxide sensor based on self-assembled graphene/polymer composite nanofibers. ACS Appl Mater Interfaces, 2014, 6: 17003–17008
12 Zhou X, Lee S, Xu Z, *et al.* Recent progress on the development of chemosensors for gases. Chem Rev, 2015, 115: 7944–8000
13 Lee JH. Gas sensors using hierarchical and hollow oxide nanostructures: Overview. Sensors Actuat B-Chem, 2009, 140: 319–336
14 Zhang J, Liu X, Neri G, *et al.* Nanostructured materials for room-temperature gas sensors. Adv Mater, 2016, 28: 795–831
15 Li J, Liu X, Cui J, *et al.* Hydrothermal synthesis of self-assembled hierarchical tungsten oxides hollow spheres and their gas sensing properties. ACS Appl Mater Interfaces, 2015, 7: 10108–10114
16 Wang L, Zhang R, Zhou T, *et al.* Concave Cu_2O octahedral nanoparticles as an advanced sensing material for benzene (C_6H_6) and nitrogen dioxide (NO_2) detection. Sensors Actuat B-Chem, 2016, 223: 311–317
17 Zhang J, Zeng D, Zhu Q, *et al.* Effect of nickel vacancies on the room-temperature NO_2 sensing properties of mesoporous NiO nanosheets. J Phys Chem C, 2016, 120: 3936–3945
18 Li Y, Zu B, Guo Y, *et al.* Surface superoxide complex defects-boosted ultrasensitive ppb-level NO_2 gas sensors. Small, 2016, 12: 1420–1424
19 Yang Y, Tian C, Wang J, *et al.* Facile synthesis of novel 3D nanoflower-like Cu_xO/multilayer graphene composites for room temperature NO_x gas sensor application. Nanoscale, 2014, 6: 7369–7378
20 Deng S, Tjoa V, Fan HM, *et al.* Reduced graphene oxide conjugated Cu_2O nanowire mesocrystals for high-performance NO_2 gas sensor. J Am Chem Soc, 2012, 134: 4905–4917
21 Zhang J, Liu J, Peng Q, *et al.* Nearly monodisperse Cu_2O and CuO nanospheres: preparation and applications for sensitive gas sensors. Chem Mater, 2006, 18: 867–871
22 Wan P, Yang W, Wang X, *et al.* Reduced graphene oxide modified with hierarchical flower-like $In(OH)_3$ for NO_2 room-temperature sensing. Sensors Actuat B-Chem, 2015, 214: 36–42
23 Kim DY, Kim CW, Sohn JH, *et al.* Ferromagnetism of single-crystalline Cu_2O induced through poly(*N*-vinyl-2-pyrrolidone) interaction triggering d-orbital alteration. J Phys Chem C, 2015, 119: 13350–13356
24 Liu X, Wang A, Li L, *et al.* Structural changes of Au–Cu bimetallic catalysts in CO oxidation: *In situ* XRD, EPR, XANES, and FT-IR characterizations. J Catal, 2011, 278: 288–296
25 Sekhar H, Narayana Rao D. Preparation, characterization and nonlinear absorption studies of cuprous oxide nanoclusters, microcubes and micro-particles. J Nanopart Res, 2012, 14: 976
26 Yang J, Zhao Y, Zhang J, *et al.* Removal of elemental mercury from flue gas by recyclable $CuCl_2$ modified magnetospheres catalyst from fly ash. Part 3. Regeneration performance in realistic flue gas atmosphere. Fuel, 2016, 173: 1–7
27 Teo JJ, Chang Y, Zeng HC. Fabrications of hollow nanocubes of Cu_2O and Cu *via* reductive self-assembly of CuO nanocrystals. Langmuir, 2006, 22: 7369–7377
28 Zhang DF, Zhang H, Guo L, *et al.* Delicate control of crystallographic facet-oriented Cu_2O nanocrystals and the correlated adsorption ability. J Mater Chem, 2009, 19: 5220–5225
29 Kruk M, Jaroniec M. Gas adsorption characterization of ordered organic–inorganic nanocomposite materials. Chem Mater, 2001, 13: 3169–3183
30 Wang Y, Lü Y, Zhan W, *et al.* Synthesis of porous Cu_2O/CuO cages using Cu-based metal–organic frameworks as templates and their gas-sensing properties. J Mater Chem A, 2015, 3: 12796–12803
31 Azimi H, Kuhri S, Osvet A, *et al.* Effective ligand passivation of Cu_2O nanoparticles through solid-state treatment with mercaptopropionic acid. J Am Chem Soc, 2014, 136: 7233–7236
32 Ghijsen J, Tjeng LH, van Elp J, *et al.* Electronic structure of Cu_2O and CuO. Phys Rev B, 1988, 38: 11322–11330
33 Zhao YM, Zhu YQ. Room temperature ammonia sensing properties of W18O49 nanowires. Sensors Actuat B-Chem, 2009, 137: 27–31
34 Chen H, Zhou S, Han Z, *et al.* A copper-based sorbent with oxygen-vacancy defects from mechanochemical reduction for carbon disulfide absorption. J Mater Chem A, 2016, 4: 17207–17214
35 Zhang L, Cui Z, Wu Q, *et al.* Cu_2O–CuO composite microframes with well-designed micro/nano structures fabricated *via* controllable etching of Cu_2O microcubes for CO gas sensors. CrystEngComm, 2013, 15: 7462–7467
36 Yang Y, Xu D, Wu Q, *et al.* Cu_2O/CuO bilayered composite as a high-efficiency photocathode for photoelectrochemical hydrogen evolution reaction. Sci Rep, 2016, 6: 35158

Acknowledgements This work was supported by the National Natural Science Foundation (51501010, 91323301, 51631001, 51372025 and 21643003). Prof. Shaohua Shen's group from Xi'an Jiaotong University is acknowledged for their support in the electron paramagnetic resonance (EPR) measurements.

Author contributions Li S and Wang M designed and engineered the samples and performed the experiments; Li C, Xu M and Liu J performed the data analysis; Liu JJ organized the paper; Zhang J and Liu JJ conceived this study. All authors contributed to the general discussion. All authors have given approval to the final version of the manuscript.

Conflict of interest The authors declare no conflict of interest.

Supplementary information Supporting materials are available in the online version of the paper.

Siyuan Li was born in Henan, China, in 1992. He received his BSc degree in 2016 from Zhengzhou University and is now studying in Beijing Institute of Technology for his MSc degree. His research interest focuses on metal oxide nanostructure and their gas sensor properties.

Mengting Wang was born in Henan, China, in 1990. She received her master degree in 2016 from the School of Materials Science & Engineering of Beijing Institute of Technology. Her research interest focuses on metal oxide nanostructure and their gas sensor properties.

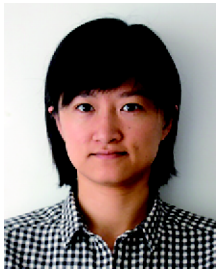

Jiajia Liu received her PhD degree in 2010 from the Department of Chemical & Biomolecular Engineering of National University of Singapore, Singapore. Currently she is an assistant professor in the School of Materials and Engineering, Beijing Institute of Technology, China. Her currently research interests include the development of metal/semiconductor composite nanostructures and their applications in sensor, catalysis, optoelectronics and biology.

Jiatao Zhang was born in 1975. He earned his PhD in 2006 from the Department of Chemistry, Tsinghua University, China. Currently he is Xu Teli Professor in School of Materials and Engineering, Beijing Institute of Technology. He was awarded Excellent Young Scientist foundation of NSFC in 2013. He also serves as the director of Beijing Key Laboratory of Construction-Tailorable Advanced Functional Materials and Green Applications. His current research interests include inorganic chemistry of semiconductor based hybrid nanostructures to possess novel optical, electronic properties for applications in energy conversion and storage, catalysis, optoelectronics and biology.

精准调控表面氧空位的Cu_xO自组装介孔微球及其室温检测NO_2的气敏性能

李思远[†], 王梦婷[†], 李朝峥, 刘佳佳[*], 徐萌, 刘佳, 张加涛[*]

摘要 本文通过简单液相方法合成了一系列可控的、不同形貌Cu_xO自组装介孔微球(病毒状、海胆状、球形). 通过改变*N*,*N*二甲基甲酰胺(DMF)溶剂中痕量水的比例, 调控Cu_xO微球形貌由球状发展为病毒状; 通过可控的化学动力学过程实现从疏松组装到紧密组装的演变. 由于其三维自组装结构, 这些Cu_xO自组装介孔微球在室温下对NO_2气体具有优良的响应特性. 结果表明, 病毒状Cu_xO自组装介孔微球在室温下对1 ppm NO_2气体具有优异的敏感特性和响应特性. 气敏机理分析发现, 其优异气敏特性来源于病毒状Cu_xO自组装介孔微球较高的比表面积、分级三维纳米结构、有效的气体扩散孔洞、表面Cu_2O/CuO的纳米异质界面以及表面有效的氧空位缺陷调控.

